Cite this article
Giongo I, Rizzi E, Riccadonna D and Piazza M
On-site testing of masonry shear walls strengthened with timber panels.
Proceedings of the Institution of Civil Engineers – Structures and Buildings,
https://doi.org/10.1680/jstbu.19.00179

Research Article
Paper 1900179
Received 04/09/2019;
Accepted 01/10/2020

Keywords: brickwork & masonry/
rehabilitation, reclamation & renovation/
timber structures

Structures and Buildings

ICE Publishing

On-site testing of masonry shear walls strengthened with timber panels

Ivan Giongo MEng, PhD
Assistant Professor, Department of Civil, Environmental and Mechanical Engineering, University of Trento, Trento, Italy
(Orcid:0000-0002-3867-2334) (corresponding author: ivan.giongo@unitn.it)

Ermes Rizzi MEng, PhD
PhD Fellow, Department of Civil, Environmental and Mechanical Engineering, University of Trento, Trento, Italy

Daniele Riccadonna MEng
PhD Candidate, Department of Civil, Environmental and Mechanical Engineering, University of Trento, Trento, Italy

Maurizio Piazza MEng
Professor, Department of Civil, Environmental and Mechanical Engineering, University of Trento, Trento, Italy (Orcid:0000-0001-6279-4860)

The effectiveness of a method to strengthen/repair unreinforced masonry (URM) by using timber-based products was investigated through experimental in situ testing. The strategy consists of timber-based panels connected to the masonry by means of screw fasteners. URM piers obtained from a century-old building were subjected to in-plane semi-cyclic quasi-static loading in as-built, repaired and retrofitted configurations. The application of the reinforcement on previously damaged piers led to a notable increase in the in-plane capacity while the initial stiffness of the repaired specimens was found to be consistent with that of the specimens tested as-built. When applied to undamaged masonry, the retrofit system allowed an in-plane force 40% higher than the capacity of the unreinforced walls, with the initial stiffness comparable with that of the repaired specimens. Both repaired and retrofitted specimens exhibited remarkable displacement capacity (drift levels > 2.0%) and energy dissipation.

1. Introduction

Unreinforced masonry (URM) is one of the most common construction typologies, and can be encountered in old town and city centres all around the world. URM construction techniques can differ but they all have limited tensile strength, which contributes to the vulnerability of URM walls to lateral loading. Over the years, a large variety of techniques aimed at improving the in-plane and out-of-plane behaviour of URM walls have been proposed (Bhattacharya *et al*., 2014; Goodwin *et al*., 2011; Wang *et al*., 2018). Such techniques rely on different strengthening materials, from steel (Borri *et al*., 2010; Corradi *et al*., 2018; Ferretti and Pascale, 2019) and concrete (Deng *et al*., 2019; Lin *et al*., 2014, 2016) to textile-reinforced mortar (De Santis *et al*., 2018; Facconi *et al*., 2014; Gattesco *et al*., 2015; Kouris and Triantafillou, 2018) and fibre-reinforced polymers (Babatunde, 2017; Dizhur *et al*., 2014). Recently, the use of timber-based materials for the retrofitting of URM buildings has attracted considerable interest due to the increasing availability of highly engineered wood products (e.g. cross-laminated timber (CLT) and laminated veneer lumber (LVL)) and the reduced environmental impact of timber with respect to other materials (Robertson *et al*., 2012). In this context, research and practice have mainly focused on two alternative concepts: (*a*) using timber structures to partially or completely supersede the masonry role in bearing vertical and/or horizontal loads (APA, 2015; De Boer, 2009) and (*b*) using timber components (e.g. timber beams/studs or panels) coupled to the masonry by means of adequate connections to form a composite system with improved in-plane and/or out-of-plane performance. Among the first examples of timber used to retrofit existing buildings, Sustersic and Dujic (2014) proposed to strengthen reinforced concrete (RC) frames with masonry infills using CLT panels connected either to the RC frame or directly to the masonry infills. Lucchini *et al*. (2014) focused on the thermal, hygrometric and acoustic performance analysis of a similar technique for the reinforcement of URM building façades. More recently, Giaretton *et al*. (2017) and Dizhur *et al*. (2017) investigated the use of timber strong-backs connected to URM walls by screw-ties with the goal of improving the out-of-plane behaviour of the walls when subjected to seismic loading. A similar retrofitting technique based on the use of strong-backs connected to existing URM walls was investigated by shake table testing by Miglietta *et al*. (2019).

Within this framework, the current authors contributed by proposing a strengthening solution for URM structures based on the use of timber panels fixed to the internal side of masonry walls by means of point-to-point dry connections. This technique is intended to improve both the out-of-plane and in-plane wall response. The work first focused on the in-plane wall performance and proceeded to numerical modelling (Giongo *et al*., 2017) and experimental shear testing of selected connections (Riccadonna *et al*., 2019). The next step of the research – on-site experimental characterisation of the retrofitting technique – is presented in this paper. Three full-scale brick masonry wall specimens were subjected to in-plane semi-cyclic loading. Two of the specimens were tested before (as-built configuration) and after (repaired configuration) applying the reinforcement panel to the wall, while the third specimen was tested with a timber panel connected to an undamaged wall (retrofit configuration).

2. Retrofitting technique

As already briefly mentioned, the proposed retrofit technique consists of timber-based panels (e.g. CLT, LVL) fixed to existing masonry walls using point-to-point connections to form a composite structural system in which the timber and masonry components collaborate with each other to resist inertial forces. The timber-to-masonry connection is realised by means of dowel-type fasteners (Riccadonna *et al.*, 2019) uniformly spread on the wall's surface. To prevent rocking of the timber panel, hold-down elements can be used to increase the system efficacy in transferring uplift forces to the ground. The system is intended for application on the internal side of walls in order to achieve better durability and preserve the building's external façades. In addition to the distributed fasteners connecting the timber panels to the masonry walls, direct diaphragm-to-timber panel connections can be adopted to further improve the box-like response of the whole building. Thanks to its reversibility, ease of implementation and speed of assembly, the proposed system can also be used in fast interventions to strengthen moderately damaged buildings in post-earthquake scenarios.

3. In situ experimental campaign

Three clay-brick wall specimens were isolated from the structure of a decommissioned hotel located in northern Italy within the Comano Terme bath area. The building, currently scheduled for demolition, was constructed in the second half of the nineteenth century as a three-storey stone masonry building, to which an extra clay-brick storey was later added on top. The floor structure is mostly of timber with a few occasional floor bays where the original wooden floor has been replaced over the years by a concrete slab. A roof structure composed of timber trusses and wooden ceilings completes the building. Wall specimens 1 and 2 were first tested in the as-built condition (AsB-1 and AsB-2) and then re-tested after being repaired (RP-1 and RP-2). By contrast, specimen 3 was tested only once, with the reinforcement applied to the undamaged and 'never before tested' specimen (R-3).

3.1 Materials

The three specimens were obtained from the internal walls of the clay-brick vertical addition constructed in the 1920s. The walls had an average thickness of 340 mm and consisted of three-leaves of masonry built with clay bricks ($\approx 200 \times 100 \times 50$ mm) and lime mortar. Prior to the wall testing, brick and mortar samples were extracted and subjected to destructive testing in the lab. Sampling was carefully executed using manual tools while taking great care to minimise disturbance of the specimens. The mechanical properties of the brick, obtained in accordance with ASTM C67 (ASTM, 2017), are provided in Table 1.

Because of a certain variability in the bed-joint thickness ($\approx$15 mm on average) and due to difficulties in removing undisturbed samples, the mortar samples were inevitably characterised by different sizes and shapes, with the smallest dimension (i.e. height of the sample) being typically that in the direction along the joint thickness.

Once extracted, the irregular samples were cut to create approximate prisms (Valek and Veiga, 2005) and a thin layer of dental stone plaster (compressive strength $>$30 MPa after 24 h) was applied to the base surfaces to favour load distribution. The value of the modulus elasticity given in Table 2 represents the secant modulus of elasticity measured between 0.1 and 0.4 of the maximum load. Estimating the compressive strength of historic mortars from irregular, small-size samples can be quite challenging due to a noticeable dependency of the results on sample size and geometry (Drdácký, 2007, 2011). However, Lumantarna (2012) proposed a series of modification factors to account for sample size/footprint, aspect ratio of the base surface and slenderness (i.e. height/base), and the adoption of such modification factors should result in

Table 1. Mechanical properties of bricks from extracted samples

Property	Number of samples	Mean	Coefficient of variation
Compressive strength, f_{bc}: N/mm^2	15	14.83	0.32
Modulus of elasticity, E_{bc}: N/mm^2	15	1225	0.29
Bending tensile strength, f_{bt}: N/mm^2	7	3.70	0.43

Table 2. Mechanical properties of mortar from extracted samples

Property	Number of samples	Mean	Coefficient of variation
Modulus of elasticity, E_{mc}: N/mm^2	13	97.9	0.30
Compressive strength, f_{mc}: N/mm^2	15	4.59[a]	0.54
		2.99[b]	0.70

[a]Value estimated using the procedure proposed by Lumantarna (2012)
[b]Value estimated using the relations derived by Drdácky *et al.* (2008)

compressive strength values consistent with those obtainable from 50 × 50 × 50 mm standard-size specimens (ASTM, 2013). As shown in Table 2, the mean compressive strength of the extracted mortar samples (obtained through normalisation) was 4.59 MPa, which exceeded that commonly expected for lime mortars (<3–4 MPa). It is worth noting that the results were affected by a large scatter and that the lower bound (i.e. mean value minus one standard deviation) was 2.11 MPa. Alternatively, using the slenderness–compressive strength relations derived by Drdácky *et al*. (2008) for square-shaped lime mortar samples, the mean compressive strength was reduced to 2.99 MPa (Table 2), with a lower bound of 0.89 MPa.

For the tests on repaired and retrofitted walls, three-layer 60 mm thick CLT panels were used. The mechanical properties of the timber panels as provided in the product standard (OIB, 2018) are shown in Table 3.

The distributed timber panel-to-masonry wall connection was realised with two different types of timber–masonry screw fasteners, shown in Figure 1. The type A fastener was a partially threaded screw intended for use in concrete and masonry. The type B fastener featured two threaded parts – a longer front thread to be inserted into masonry and a shorter rear thread to be inserted into timber. To increase the contact surface between the screw head and the panel, type A fasteners were installed with ∅43 mm washers. The characteristics of the fasteners are provided in Table 4. The mechanical properties of the type A fasteners were taken from the available product standard (DIBt, 2015), while the properties of the type B fasteners were obtained experimentally (BSI, 2016). An 8 mm thick steel bracket (UPN profile) fixed to the CLT panel by using 13 screws (∅8 mm × 80 mm) was used as hold-down to prevent panel uplift (Figure 2). A 16 mm steel threaded rod anchored the bracket to the floor structure. The bracket capacity was designed to provide sufficient over-strength so as not to experience hold-down failure during testing.

3.2 Specimen preparation

After removal of the original plaster, three wall portions of 1800 mm × 1800 mm were isolated from the surrounding masonry by through-cutting the walls with a circular steel blade with diamond segments (Figure 3(a)). The weight of the roof, the uppermost floor and the masonry above the horizontal cuts was supported on provisional steel props to guarantee safety, as shown in Figure 3(b). Vertical load simulating the vertical stress at the base of a three-storey building (assumed to

Table 3. Mechanical properties of spruce CLT panels (in-plane wall behaviour)

	Value
Bending strength, $f_{m,k}$: N/mm^2	24
Tensile strength parallel to grain, $f_{t,0,k}$: N/mm^2	14.5
Tensile strength perpendicular to grain, $f_{t,90,k}$: N/mm^2	0.12
Compressive strength parallel to grain, $f_{c,0,k}$: N/mm^2	21
Compressive strength perpendicular to grain, $f_{c,90,k}$: N/mm^2	2.5
Shear strength, $f_{v,k}$: N/mm^2	2.3
Modulus of elasticity, $E_{0,mean}$: N/mm^2	11550
Shear modulus, G_{mean}: N/mm^2	450
Mean density, ρ_{mean}: kg/m^3	420
Characteristic density, ρ_k: kg/m^3	350

Table 4. Properties of timber–masonry fasteners

	Type A	Type B[a]
Total length, L: mm	180	230
Thread length, L_t: mm	100	160 (70)
Thread diameter, d_{thread}: mm	12.0	10.0 (12.0)
Core diameter, d_{core}: mm	9.4	7.5
Shaft diameter, d_{shaft}: mm	9.4	—
Hole diameter, d_{hole}: mm	10	8
Axial resistance[b], N_{Rks}: kN	25	58
Bending resistance[b], M_{Rks}: N.m	71	65[c]

[a]Values in brackets are timber thread properties
[b]Characteristic value
[c]Value calculated according to ETAG 001-C (EOTA, 2010)

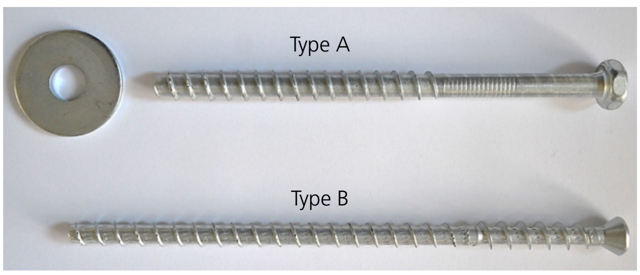

Figure 1. TM fasteners: (a) type A + washer; (b) type B

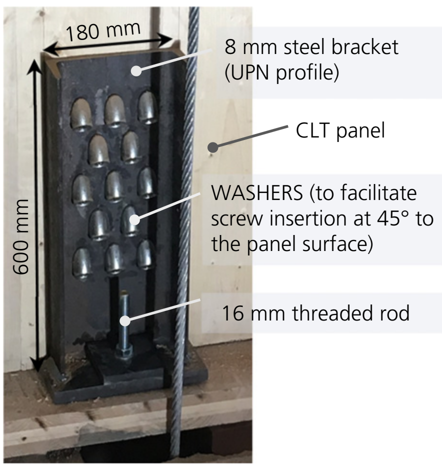

Figure 2. Steel bracket used as hold-down device

Figure 3. Specimen preparation: (a) specimen after removal of plaster and creation of through cuts; (b) specimen AsB-1 prior to testing; (c) specimen R-1 prior to testing

be ≈0.22 MPa) was applied to the top surface of the specimens using a loading rig (described in the next section). A 30 mm thick (on average) layer of lime mortar (strength class M5) was laid on top of the specimen surface to provide adequate load spreading. To prevent local crushing of the masonry due to force concentration in the area surrounding the hydraulic jack, a 250 × 250 × 15 mm steel plate was placed on top of a 20 mm thick layer of high-strength mortar. The reinforcement was installed by drilling calibrated holes through both the CLT panel and the masonry with a regular pattern according to the spacing values listed in Table 5. Spacing values were defined based on the results of previous analyses (Giongo *et al.*, 2017). Regularity of the pattern was partially altered to avoid the cracks that originated from the testing of the specimens in the as-built condition. As the masonry wall surface was hidden by the CLT panel, care was taken to drill the holes in correspondence with the bricks so as not to install fasteners into the mortar bed joints and consequently reduce their effectiveness. Holes were cleared from dust and debris prior to the fastener insertion with an impact screwdriver. The CLT panels were installed so that the grain direction of the external board layers was oriented vertically (Figure 3(c)).

3.3 Test setup and instrumentation

A schematic illustration of the test setup is shown in Figure 4(a). Vertical compression was applied to the top

Table 5. Specimen IDs and description

Test ID	Configuration	Wall thickness[a]: mm	Timber–masonry fastener	Fastener spacing[b]: mm	Reinforcement side
AsB-1	As-built	340	—	—	—
RP-1	Repaired	340	Type A	400	R
AsB-2	As-built	340	—	—	—
RP-2	Repaired	340	Type B	400	L
R-3	Retrofitted	340	Type B	300	R

[a]Wall surface area 1800 × 1800 mm^2
[b]Spacing in both horizontal and vertical directions

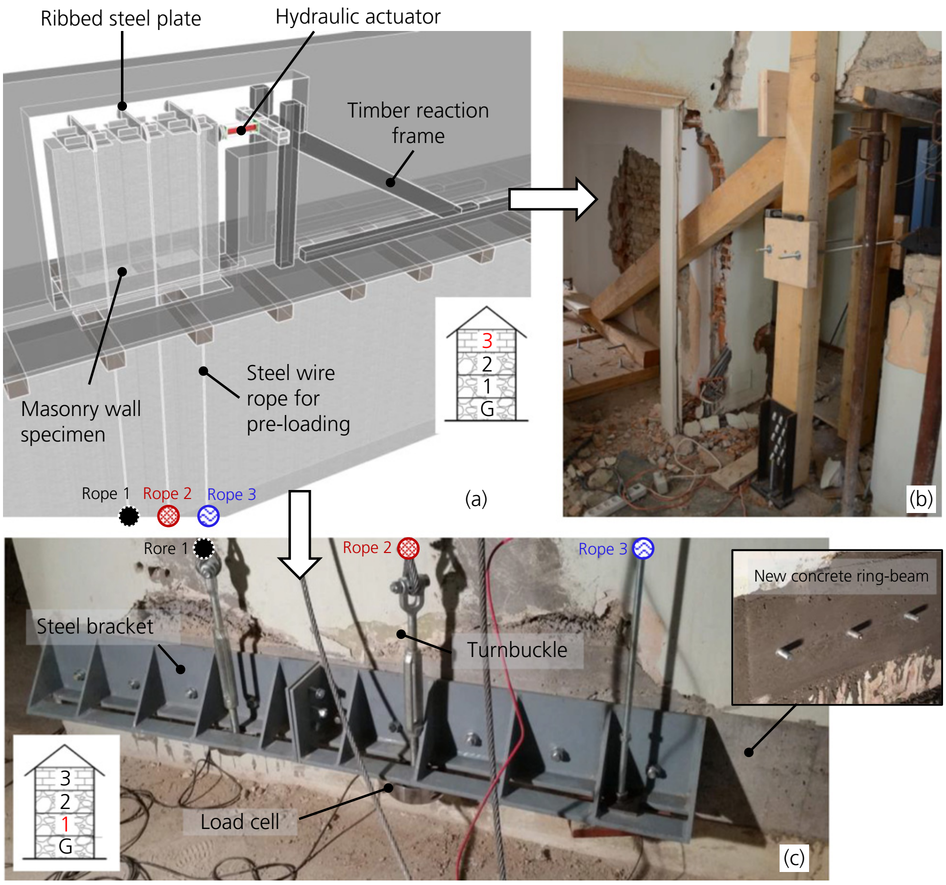

Figure 4. Test setup: (a) schematic diagram; (b) close-up of timber reaction frame; (c) details of anchoring system for the steel wire ropes

surface of the specimen by means of three steel wire ropes of diameter 14 mm. The wire ropes were anchored to RC ring beams located at the first floor level and were purposely built for this testing campaign (Figure 4(c)). Ribbed steel plates with specifically designed rounded rails to guide the wires were positioned on top of the specimen to allow force transfer from the wire ropes to the masonry. The parameter ψ (the ratio of the effective height (i.e. distance from the wall base to the point where the moment zeroed) to the specimen total height) was used to describe the wall fixity condition under lateral loading (vertical preload was assumed to be uniformly distributed). Due to the restraint effect associated with the presence of the wire ropes, ψ was calculated to be 0.82, whereas values of 0.5 and 1.0 would be expected in the case of double fixed-end and fixed-free (i.e. cantilever) conditions, respectively.

The horizontal load was applied by a single-effect hydraulic jack positioned at approximately 1600 mm from the base of the specimen. The reaction to lateral loading was provided by a horizontal steel I-beam connected to two timber frames, one on each side of the masonry wall (Figure 4(b)). The reaction frames were built using solid-wood beams and were anchored to the existing floor structure. The magnitude of the lateral force was measured by a 300 kN load cell provided with a spherical articulation for optimal force transfer. It is worth stressing that in all the tests, the horizontal force simulating earthquake action was applied to the masonry with no direct load transfer between the actuator and the CLT panel (when present).

Deformations were measured by a total of eight wire transducers, four on each side of the wall (measuring the two diagonals and the vertical tension and compression edges). The instruments were identified by means of a letter (V for vertical and D for diagonal), a number (1 for instruments expected to read elongations and 2 for shortening) and an additional letter identifying the side of the specimen with respect to the loading direction (see Figure 5).

Absolute horizontal displacements were measured by means of a linear variable differential transformer (LVDT) positioned at the actuator location and a couple of wire transducers installed at the front end of the specimen (see Figure 5). Out-of-plane displacements were monitored by means of two LVDTs placed at the front end (DISP_OF) and the rear end (DISP_OB) of the specimen.

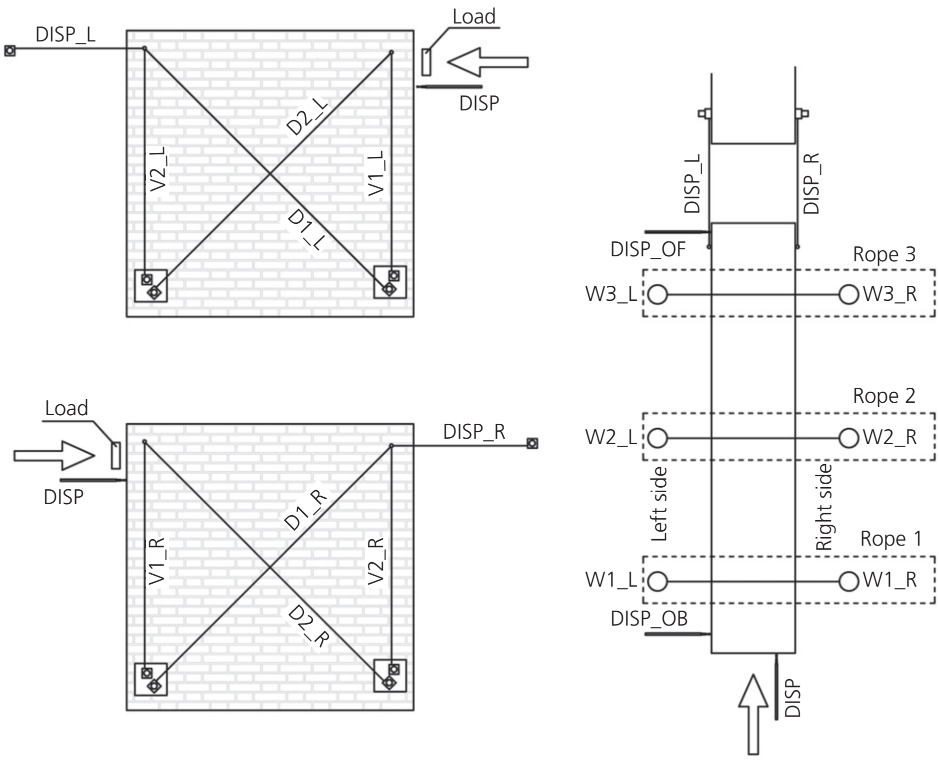

Figure 5. Instrument layout

On the reinforced side of the repaired/retrofitted specimens, wire sensors were applied to the CLT panel to measure timber in-plane deformations and absolute horizontal displacement in the direction of loading; the above-mentioned instruments recording the out-of-plane deformations were always placed on the unreinforced side of the wall. In the case of the repaired/retrofitted specimens, vertical tension force on the hold-down was measured by means of a ring load cell, while panel uplift was measured by an additional linear displacement transducer. Tension forces acting on the wire ropes were monitored by means of six load cells positioned at the rope anchoring points.

3.4 Test protocol

Vertical forces were introduced by increasingly tensioning the six ends of the wire ropes up to ≈23 kN each so as to produce a uniform compression stress over the specimen's top surface of ≈0.23 MPa (corresponding to a total force of 138 kN distributed over an area of 1800×340 mm^2). The wire ropes were tensioned by steps of 5 kN load increments starting from the central rope at every step. During application of the vertical load, data from the instruments were continuously recorded. Once the wire ropes had been tightened, shear testing began by applying load semi-cycles with the actuator acting in compression only. Due to safety requirements, the turnbuckles (Figure 4(c)) used to tighten the wire ropes were not operated once the lateral loading started and therefore adjustments to compensate for the inevitable tightening/loosening of the ropes were not possible. The variation of the vertical applied stress at cycle peak load was monitored throughout the whole testing process and it was found to be always within 10%.

To allow the specimens to be effectively repaired after testing, the loading sequences on the as-built specimens were terminated at the formation of a shear failure mechanism, evidenced by a typical stair-stepped diagonal crack, without reaching the ultimate displacement capacity. The repaired and retrofitted specimens were first subjected to force-controlled load cycles, similarly to the as-built specimens. When the applied load approached the specimen's in-plane shear capacity, load application switched to displacement control and additional cycles were performed with increasing displacement amplitudes. Further details on the test sequence are provided in the next section. The actuator was driven by a manual hydraulic pump, maintaining a displacement velocity of approximately 0.2 mm/s.

3.5 Results and discussion

The uniform vertical stresses (σ_0) applied to the specimens are listed in Table 6 along with estimations of the masonry's elastic modulus (E) obtained from data collected during the vertical loading phase. The measured elastic modulus values, even though small when compared with probable values

Table 6. Applied vertical stress (σ_0) and elastic modulus (E) of masonry wall specimens

Test ID	σ_0: MPa	E: MPa
AsB-1	0.22	381.6
RP-1	0.22	
AsB-2	0.22	239.9
RP-2	0.23	
R-3	0.21	301.0

suggested by recognised international guidelines such as those published by the New Zealand Society for Earthquake Engineering (NZSEE, 2017) and the Italian Ministry of Infrastructure and Transport (MIT, 2019) (see also Kaushik *et al.*, 2007), appear consistent with the experimental values reported by Drougkas *et al.* (2016) for air lime mortars. The small modulus of elasticity observed for the wall specimens was largely influenced by the mortar stiffness (E_{mc} = 98 MPa, Table 2). In fact, if the masonry composite was schematised by a set of linear elastic springs working in series and representing the mortar and the bricks (Drougkas *et al.*, 2016), a masonry E value of 346 MPa would be obtained for E_{mc} = 98 MPa and E_{bc} = 1225 MPa (bed-joint thickness = 15 mm and brick thickness = 53 mm).

3.5.1 Specimen 1

Subsequent to the application of vertical stress up to 0.22 MPa, specimen 1 was first tested in the as-built unreinforced condition (AsB-1). Horizontal loading was applied in semi-cycles following a stepwise procedure of 5 kN load increments up to 30 kN, after which the step size was increased to 10 kN until the maximum load (F_{max} = 69.3 kN) was reached. The failure mechanism was identified by the formation of a stair-stepped diagonal crack involving both mortar bed-joints and bricks, as illustrated in Figure 6(b). No visible cracking was observed prior to the maximum load, with the sole exception of a horizontal crack located in the mortar bed-joint at the specimen base on the wall's tension side. This horizontal crack, associated with the wall rocking response, was only visible at the cycle peaks and had a length ranging from a few centimetres to ≈20 cm at the last loading cycle. Figure 6(a) shows the load–displacement curves obtained from AsB-1 test plotted with reference to the displacements measured by the DISP_R and DISP_L transducers (shown in Figure 5).

After the formation of a diagonal crack (the sign that the maximum shear capacity of the URM specimen had been reached), the test was ended. A 60 mm thick CLT panel was then connected to the tested specimen by means of 17 type A fasteners (Table 4): 16 fasteners (≈five fasteners per square metre of wall surface area) were arranged on four rows, maintaining a minimum distance from the panel edge of approximately 300 mm and an approximate spacing of 400 mm between the fasteners (Table 5). An additional fastener was inserted near the edge of the wall to prevent the premature collapse (with consequent possible damage to the instrumentation) of a small portion of the wall isolated by the cracks from previous testing in the unreinforced condition. The load–displacement curves of the CLT panel and the masonry wall are shown in Figure 7.

The load–displacement curves and cumulative dissipated energy curves for specimen 1 are compared in Figure 8. The cumulative dissipated energy (E_d) was computed as the integral of the lateral force over the horizontal displacement at the top of the specimen. Thanks to the reinforcement, the lateral stiffness of the repaired specimen was found to be consistent with the stiffness of the undamaged wall (−1.4% variation of the secant stiffness (K_s) at $0.4F_{max}$ and $0.1F_{max}$) while the

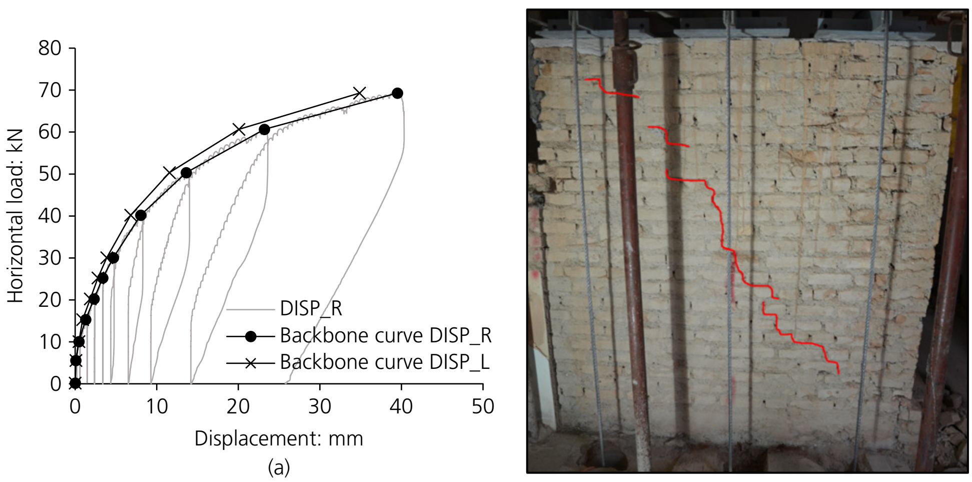

(b)

Figure 6. Specimen 1 as-built (AsB-1): (a) load–displacement curves; (b) crack pattern at peak loading

shear capacity increased significantly (+37.1% variation of maximum load F_{max}) as did the energy dissipation capacity (+86.1% of maximum E_d at the end of the last semi-cycle). For the repaired configuration, E_d was evaluated based on the displacements of the unreinforced side of the specimen only. Details of the parameters derived from the experimental curves are provided in Table 7. Figure 9 shows specimen 1 after testing.

3.5.2 Specimen 2

Test AsB-2 was carried out following the same loading procedure as for AsB-1 (i.e. 5 kN steps up to 30 kN and then 10 kN steps up to the maximum load). However, unlike in the first test, an extra load cycle was performed after the formation of the diagonal shear failure mechanism (for a shear load of approximately 70 kN, consistent with test AsB-1), pushing the specimen up to a net displacement of 50 mm at the top (Figure 10). Similarly to test AsB-1, the failure mechanism of AsB-2 was marked by the formation of a stair-stepped diagonal crack along the compressed wall diagonal, as highlighted by the crack pattern shown in Figure 10(b).

The masonry pier was then reinforced with a 60 mm thick CLT panel connected to the masonry using 16 type B fasteners (Table 4). Edge distances and fastener spacings were similar to those adopted for test RP-1, within the geometric limitations of the brick courses, by arranging the fasteners in four rows of four connectors. After repair, a 20.0% increase in the

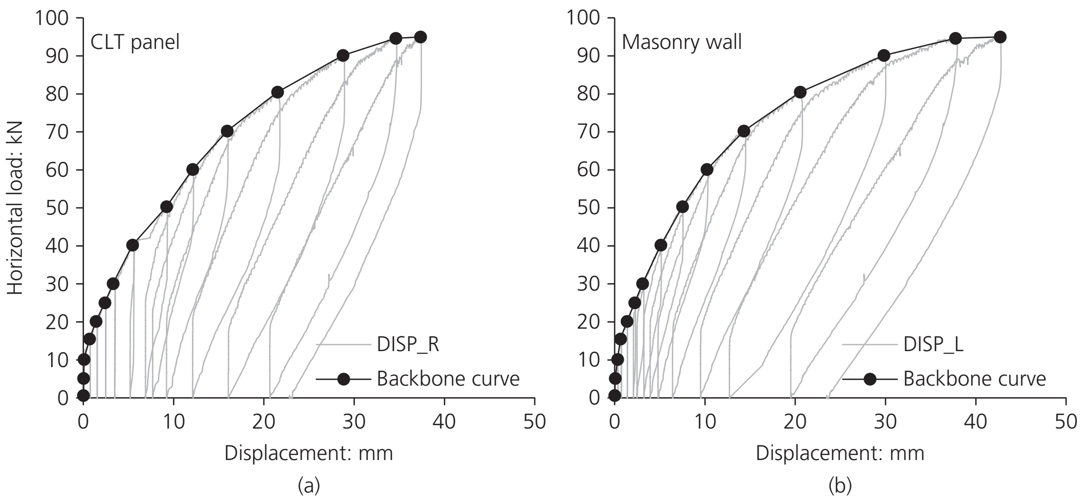

Figure 7. Load–displacement curves of repaired specimen 1 (RP-1): (a) timber panel side; (b) masonry wall side

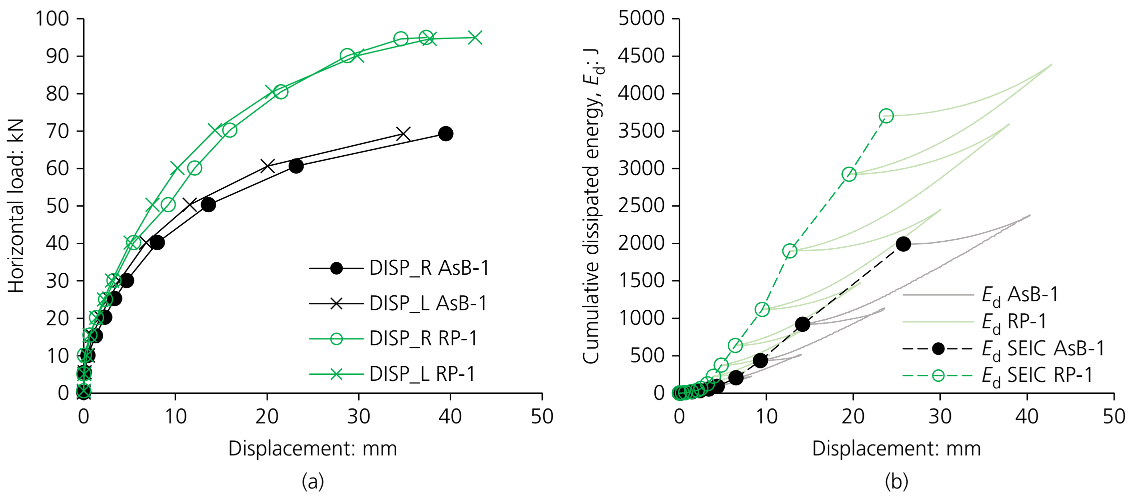

Figure 8. Specimen 1 – comparison of as-built (AsB-1) and repaired (RP-1) configurations: (a) backbone curves; (b) energy dissipation (SEIC = semi-cycle endpoint interpolation curve)

Table 7. Summary of the experimental outcomes in terms of maximum load, stiffness and dissipated energy

	Fastener							
Specimen ID	Type	Number	F_{max}: kN	K_s: kN/mm	$E_{d\ max}$: J	DR$_{max}$ [a]: %	$F_{max\ HD}$: kN	K_{HD}: kN/mm
AsB-1	—	—	69.3	6.62	1990		—	—
RP-1	A	17	95.0	6.53	3703		39.9	4.75
AsB-2	—	—	75.9	5.94	3057		—	—
RP-2	B	16	91.1	4.50	3732	2.5	32.4	3.54
R-3	B	25	106.0	5.28	7484	4.5	53.0	2.63

[a]The values refer to the maximum deformation reached during testing and might underestimate the specimen's deformation capacity

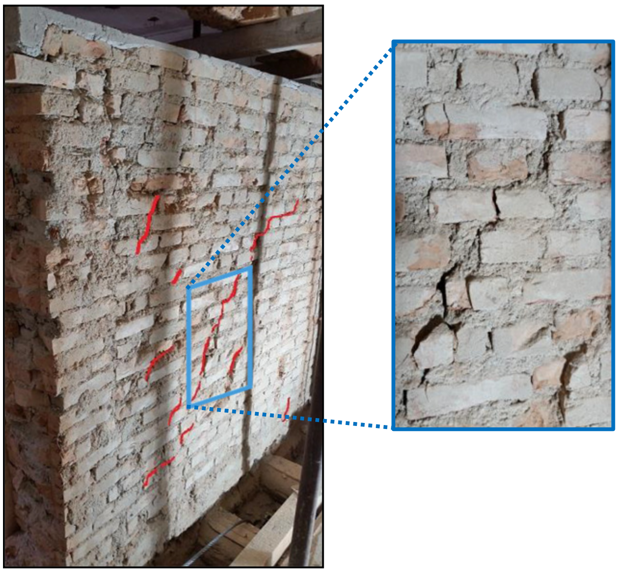

Figure 9. Specimen 1 after testing (unreinforced side)

maximum capacity (F_{max}) of specimen 2 was observed (test RP-2), with a clear 'pseudo-ductile' post-yield response. However, due to safety reasons (e.g. cracking of the masonry spandrel adjacent to the specimen base and increasing out-of-plane displacements), it was not possible to reach the ultimate deformation capacity. It is worth mentioning that the 44.7 mm displacement reached during RP-2 test by instrument DISP_R (Figure 11(a)) corresponded to a drift ratio (DR) of 2.5% (DR = displacement/wall height) that largely exceeded the acceptance criteria for ultimate limit states recommended for masonry piers by relevant standards (e.g. MIT (2019) recommends drift values at near collapse of 1.0% in the case of flexural/rocking failure and 0.5% in the case of shear failure). It is also important to note that a residual deformation from AsB-2 (characterised by a residual displacement of approximately 33 mm at the top of the wall) was present when test RP-2 was started. If such residual deformation was included in the calculation of the DR, the DR value would be 4.3%.

Due to the extensive damage experienced by specimen 2 when tested in the unreinforced condition, a reduced initial stiffness

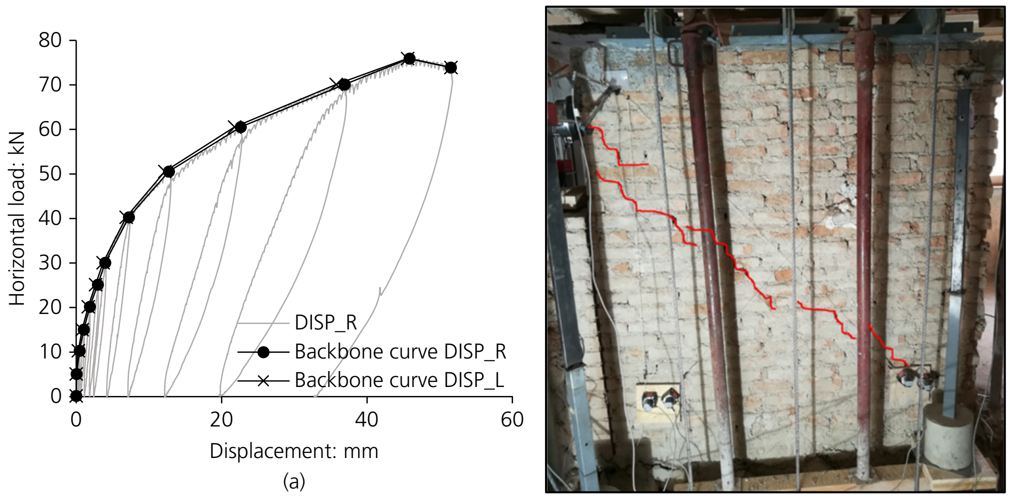

(b)

Figure 10. Specimen 2 as-built (AsB-2): (a) load–displacement curves; (b) crack pattern at peak loading

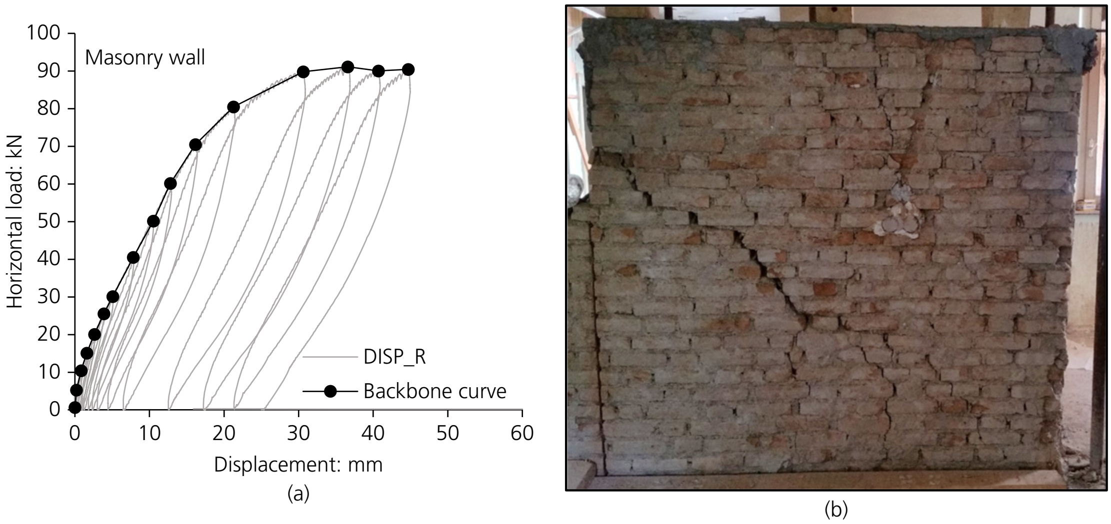

Figure 11. Specimen 2 repaired (RP-2): (a) load–displacement curve of unreinforced side; (b) specimen after testing (unreinforced side)

was observed for the repaired configuration as compared with the as-built condition (−24.2% variation of secant stiffness K_s). The increase in maximum capacity F_{max} (+20.0%) and cumulative energy dissipation E_d (+22.1%) was smaller than that observed for specimen 1, but appreciable nonetheless. It should be noted that the maximum energy dissipation (shown by the dashed curves in Figure 12(b)) was evaluated at different displacement amplitudes. If the comparison were to be made by referring to the end point of the last unloading cycle of test RP-2 for both curves (using linear interpolation for AsB-2), then the dissipated energy increase would increase to 62.5%.

3.5.3 Specimen 3

For the last test, a reinforcement panel was applied to a wall specimen that had not been previously tested in order to assess the effectiveness of the strengthening solution in a scenario without pre-existing damage. A total of 25 type B fasteners (≈eight fasteners per square metre of wall surface area) were used to connect the CLT panel to the masonry wall. The fasteners were arranged in five rows with 300 mm spacing in both vertical and horizontal directions and at a 300 mm distance from the panel edges. Figure 13 shows the loading cycles and the envelope curves plotted with respect to the displacements of the timber panel and the masonry wall. After reaching the maximum load capacity of the system at a lateral force of 106 kN, with the formation of a clear shear failure mechanism (Figure 14), additional load cycles were performed under displacement control by increasing the displacement amplitude (measured with reference to the masonry side of the specimen) by 10 mm at each cycle. As is visible in Figure 13, specimen

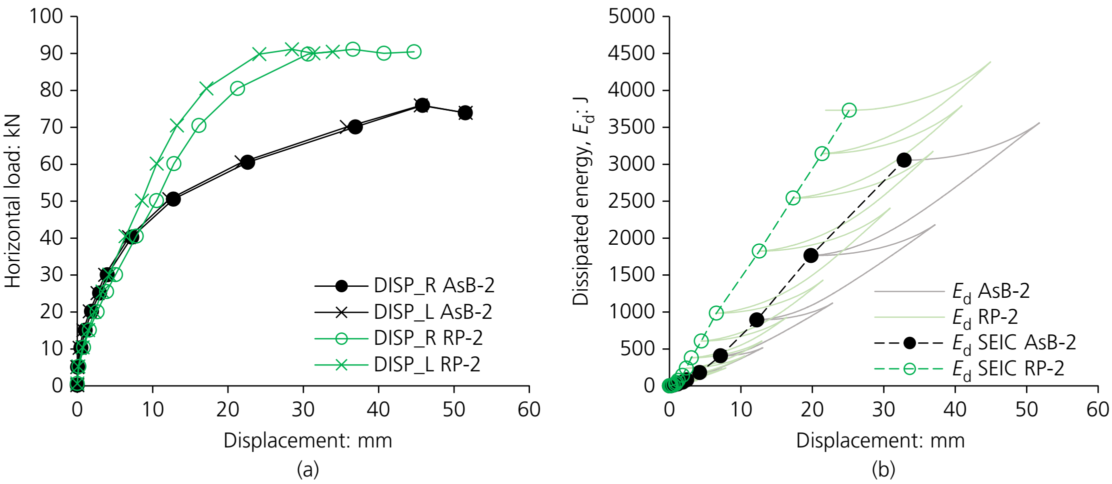

Figure 12. Specimen 2: comparison of as-built (AsB-2) and repaired (RP-2) configurations: (a) backbone curves; (b) energy dissipation (SEIC = semi-cycle endpoint interpolation curve)

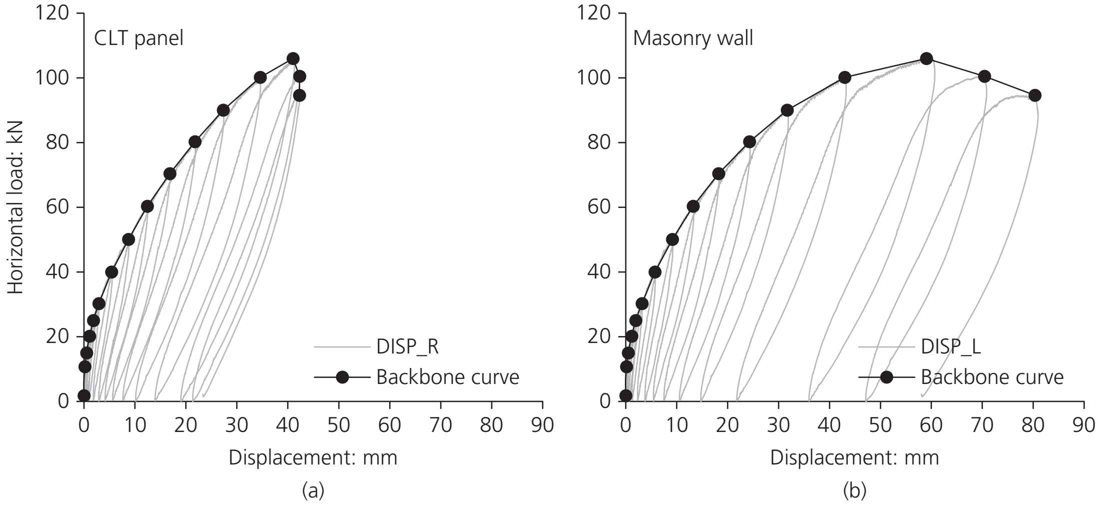

Figure 13. Load–displacement curves of retrofitted specimen 3 (R-3): (a) timber panel side; (b) masonry wall side

Figure 14. Damage to specimen R-3: (a) diagonal shear crack formation at peak loading; (b) crack pattern at the end of testing

R-3 exhibited a softening behaviour with a 10% capacity loss after two cycle sets under displacement control (maximum wall displacement of 80.3 mm). Similar to the tests on specimen 2, it was not possible to reach the ultimate capacity of specimen 3 due to safety concerns. However, the observed experimental drift capacity was equal to DR = 4.5% (at peak loading DR = 3.3%), denoting a remarkable deformation capacity of the strengthened system. The portion of drift capacity associated with the shear deformation (DR_{shear}) was calculated from the readings of the instruments located at the specimen diagonals and corresponded to $DR_{shear} = 3.1\%$ (at peak loading $DR_{shear} = 1.6\%$). Morandi *et al.* (2018) report details of the expected deformation capacity of unreinforced brick walls: based on the analysis of a dataset of 30 solid clay-brick walls from various testing campaigns reported in the literature, Morandi *et al.* (2018) suggest different drift values in relation to the failure mode. Specifically, the mean drift values at peak loading and at maximum measured displacement are, respectively, 0.39% and 1.45% for flexural failures and 0.26% and 0.46% for shear failures.

3.5.4 General remarks

The load–displacement and energy dissipation curves from all the tests are compared in Figure 15. To allow a direct

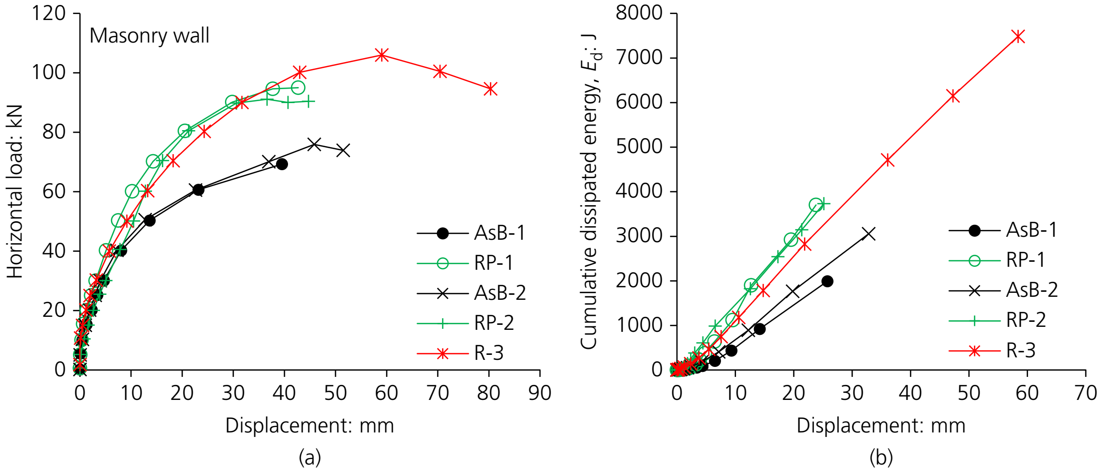

Figure 15. Comparison of the load–displacement backbone curves (a) and energy dissipation (b) for every test performed

comparison between the as-built and repaired/retrofitted test configurations, the displacement values were taken from the instruments fixed to the masonry. A remarkable consistency can be observed between the responses of AsB-1 and AsB-2, making it plausible to assume that specimen 3 would also have shown similar behaviour if tested in the as-built condition. Consequently, it appears reasonable to conclude that, thanks to the strengthening intervention, the shear capacity of specimen 3 (test R-3) was increased by 40%. When used to repair previously damaged walls (tests RP-1 and RP-2), the proposed technique not only permitted restoration of the original shear capacity of the wall but also resulted in a noticeable capacity increase ($\geq$20%). As shown in Table 7, all the tested configurations (as-built, repaired and retrofitted) exhibited comparable stiffness values. The lack of any noticeable stiffness increase due to the strengthening (compare R-3 with AsB-1 and As-B-2) together with the increase in shear capacity shown by the repaired specimens (RP-1 and RP-2) seem to confirm the findings of a previous numerical study (Giongo *et al.*, 2017) that suggest that the reinforcement system is effectively engaged only after cracking of the wall. Such a negligible impact on wall stiffness could prove beneficial to the applicability of the strengthening technique as it could be adopted to strengthen only a few selected wall piers without the risk of major changes in the force distribution within the building, as opposed to alternative and popular strengthening techniques such as jacketing of walls with shotcrete.

Table 7 also lists the maximum force ($F_{\text{max HD}}$) and the stiffness (K_{HD}) of the hold-downs used to anchor the timber

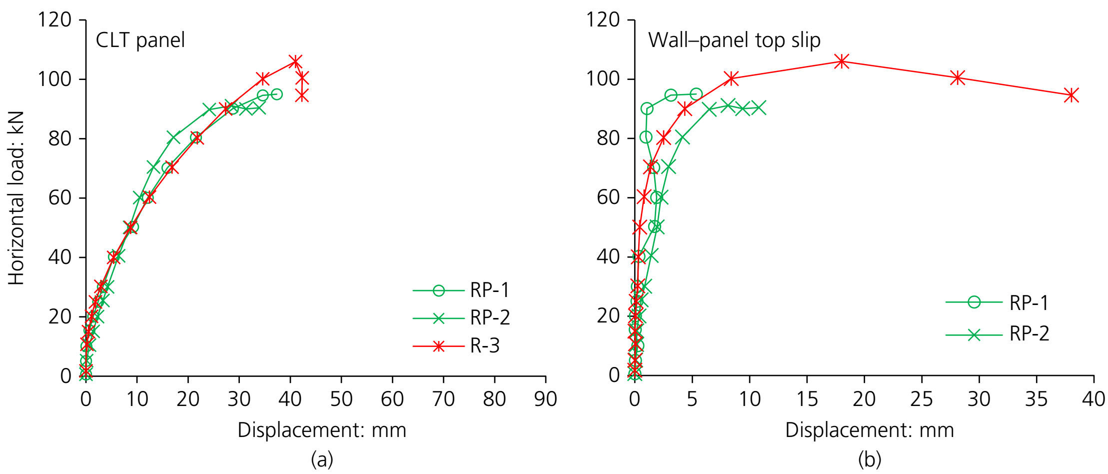

Figure 16. (a) Comparison of backbone curves obtained from CLT panel readings. (b) Masonry wall–CLT panel slip measured at top of specimen

(a) (b)

Figure 17. Fastener deformation observed from specimen R3: (a) residual fastener deformation after extraction; (b) local timber bearing failure

panels to the floor. The different hold-down stiffnesses exhibited by the three specimens reflect the different anchoring conditions. The higher value measured for specimen 1 was due to the nearby presence of a RC floor, which allowed for a stiffer connection. For the other two specimens, the hold-down was anchored to wood joists as the closest floor structure was a timber floor. It is worth noting that the hold-down performance derived from the data shown in Table 7 appears to be fully compatible with the capacity and stiffness of devices already on the market (Acler *et al.*, 2011; Gavric *et al.*, 2014; Tomasi and Sartori, 2013).

Figure 16 shows the backbone curves with reference to the measurements taken on the timber panels (Figure 16(a)) and the slip values measured at the masonry-to-timber interface at the top of the specimen (Figure 16(b)). When the lateral load approached the specimen's peak capacity, the wall–panel slip increased, indicating progressive yielding of the fasteners (approximately at slip values of 5–10 mm in accordance with previous works by the authors (Riccadonna *et al.*, 2019)). This was particularly evident for specimen 3, where the reinforced wall was tested up to a maximum displacement of 80 mm while the CLT panel experienced only half of the displacement.

To ensure the effective transfer of vertical loads from the roof to the lower levels after the removal of the provisional steel props at the end of the testing campaign, the wall specimens and the CLT panels had to remain in place after testing and load continuity had to be restored. Therefore, only a small number of fasteners could be extracted. The unscrewing process inevitably resulted in partial straightening of the fasteners during extraction, which did not allow for precise measurement of the fastener's deformation. Nonetheless, evidence of fastener yielding is visible from Figure 17(a), which shows a fastener extracted from specimen 3. Local bearing failure of the timber in the proximity of the fastener head was also observed (Figure 17(b)).

4. Conclusions

The outcomes of an in situ experimental campaign to investigate the effectiveness of a technique for repairing and retrofitting URM walls by using CLT panels have been presented. The main results, which appear quite promising, can be summarised as follows.

- Damaged specimens showed shear capacities greater than the original wall capacity ($\geq +20\%$) after being repaired with CLT panels connected to the masonry through a minimum of about five screw fasteners per square metre of wall surface. Specimen performance showed limited sensitivity to the typology and diameter of the screw fasteners.
- In the case of retrofits, the specimen capacity was observed to be a remarkable 40% higher than the capacity of similar unreinforced specimens, thanks to the use of about eight screw fasteners per square metre of wall surface. Pronounced yielding of the fasteners was observed after wall cracking.
- Although it was not possible to reach ultimate displacements of the specimens, the displacement capacity shown by both repaired and retrofitted specimens was significantly larger than the values recommended by current standards for the ultimate limit state. In particular, retrofitted test R3 showed a notable drift capacity of 4.5%.
- Reinforced wall specimens tested in either repaired or retrofitted configurations showed energy dissipation levels significantly higher than those observed for the specimens tested as-built.
- The test results showed a negligible impact of the reinforcement on the wall lateral stiffness, confirming that the reinforcement system was effectively engaged only after wall cracking. Because of this, selective wall strengthening can be applied without significant alterations of the force distribution among the resisting walls of the building.
- The good performance shown by the repaired and retrofitted specimens was obtained with the CLT panels anchored to the ground by means of hold-downs that inhibited rocking of the panel. The strength and stiffness demands on the hold-down were found to be compatible with the performance of commercial devices commonly used in the field of timber construction.

Acknowledgements

This research work was carried out within the framework of the 2019–2021 ReLUIS-DPC network (Italian University

Network of Seismic Engineering Laboratories and Italian Civil Protection Agency). The authors most gratefully thank the Terme di Comano (IT) thermal consortium for kindly providing access to the building and for allowing the experimental campaign to be undertaken. Terremoto Ltd, Rubner Holzbau S.r.l. and HECO Italia EFG S.r.l., are gratefully acknowledged for supporting the research and for supplying the fasteners and the timber material required to repair and strengthen the masonry wall specimens.

REFERENCES

Acler E, Piazza M, Tomasi R and Webber M (2011) Experimental investigation of the behaviour of different types of connections between the XLAM panels and the concrete slab. *Proceedings of Structural Engineering World Congress SEWC 2011, Como, Italy.*

APA (The Engineered Wood Association) (2015) *Robust Glulam Frame Supports Historic Building Renovation in Newport, RI.* APA, Tacoma, WA, USA.

ASTM (2013) C109: Standard test method for compressive strength of hydraulic cement mortars. ASTM International, West Conshohocken, PA, USA.

ASTM (2017) C67: Standard test methods for sampling and testing brick and structural clay tile. ASTM International, West Conshohocken, PA, USA.

Babatunde SA (2017) Review of strengthening techniques for masonry using fiber reinforced polymers. *Composite Structures* **161**: 246–255, https://doi.org/10.1016/j.compstruct.2016.10.132.

Bhattacharya S, Nayak S and Dutta SC (2014) A critical review of retrofitting methods for unreinforced masonry structures. *International Journal of Disaster Risk Reduction* **7**: 51–67, https://doi.org/10.1016/J.IJDRR.2013.12.004.

Borri A, Corradi M, Speranzini E and Giannantoni A (2010) Reinforcement of historic masonry with high strength steel cords. *Masonry International* **23(3)**: 79–90.

BSI (2016) BS EN ISO 6892-1:2016: Metallic materials. Tensile testing. Method of test at room temperature. BSI, London, UK.

Corradi M, Di Schino A, Borri A and Ruffini R (2018) A review of the use of stainless steel for masonry pier repair and reinforcement. *Construction and Building Materials* **181(3)**: 335–346, https://doi.org/10.1016/j.conbuildmat.2018.06.034.

De Boer J (2009) *Reanimation of Ruins.* Pop-up City, Amsterdam, the Netherlands. See https://popupcity.net/observations/reanimation-of-ruins/ (accessed 20/10/2020).

De Santis S, De Canio G, de Felice G *et al.* (2018) Seismic out-of-plane vertical bending behaviour of masonry walls reinforced with textile reinforced mortars. *Proceedings of the 10th International Masonry Conference, Milan, Italy* (Milani G, Taliercio A and Garrithy S (eds)). International Masonry society, pp. 1045–1055.

Deng M, Dong Z and Ma P (2019) Cyclic loading tests of flexural-failure dominant URM walls strengthened with engineered cementitious composite. *Engineering Structures* **194**: 172–182.

DIBt (Deutsches Institut fur Bautechnik) (2015) *ETA-05/0010: HECO MULTI-MONTI MMS. Concrete Screw for use in Concrete.* DIBt, Berlin, Germany.

Dizhur D, Griffith MC and Ingham JM (2014) Out-of-plane strengthening of unreinforced masonry walls using near surface mounted fibre reinforced polymer strips. *Engineering Structures* **59**: 330–343.

Dizhur D, Giaretton M, Giongo I and Ingham J (2017) Seismic retrofit of masonry walls using timber strong-backs. *SESOC Journal* **30(2)**: 30–44.

Drdácký M (2007) Testing of historic mortars on non-standard small size specimens. In *In situ Evaluation & non-Destructive Testing of Historic Wood and Masonry Structures* (Binda L, Drdácký M and Praha KB (eds)). RILEM Publications, Bagneux, France, pp. 130–139.

Drdácký M (2011) Non-standard testing of mechanical characteristics of historic mortars. *International Journal of Architectural Heritage* **5(4–5)**: 383–394, https://doi.org/10.1080/15583051003717788.

Drdácky M, Mašín D, Mekonone MD and Slížková Z (2008) Compression tests on non-standard historic mortar specimens. In *Proceedings of Historical Mortar Conference, Lisbon, Portugal.*

Drougkas A, Roca P and Molins C (2016) Compressive strength and elasticity of pure lime mortar masonry. *Materials and Structures* **49**: 983–999, https://doi.org/10.1617/s11527-015-0553-2.

EOTA (European Organization for Technical Approvals) (2010) ETAG 001: Guideline for European technical approval of metal anchors for use in concrete – Annex C: Design methods for anchorages. EOTA, Brussels, Belgium.

Facconi L, Conforti A, Minelli F and Plizzari GA (2014) Improving shear strength of unreinforced masonry walls by nano-reinforced fibrous mortar coating. *Materials and Structures* **2014**: 18, https://doi.org/10.1617/s11527-014-0337-0.

Ferretti E and Pascale G (2019) Combined strengthening techniques to improve the out-of-plane performance of masonry walls. *Materials* **12(7)**: 1171, https://doi.org/10.3390/ma12071171.

Gavric I, Fragiacomo M and Ceccotti A (2015) Cyclic behaviour of typical metal connectors for cross-laminated (CLT) structures. *Materials and Structures* **48**: 1841–1857, https://doi.org/10.1617/s11527-014-0278-7.

Gattesco N, Amadio C and Bedon C (2015) Experimental and numerical study on the shear behaviour of stone masonry walls strengthened with GFRP reinforced mortar coating and steel-cord reinforced repointing. *Eng Struct* **90**: 143–157.

Giaretton M, Ingham JM and Dizhur D (2017) Timber strong-backs as cost-effective seismic retrofit method for URM buildings. *Proceedings of the 2017 New Zealand Society for Earthquake Engineering (NZSEE) Annual Conference, Wellington, New Zealand.*

Giongo I, Schiro G and Piazza M (2017) On the use of timber-based panels for the seismic retrofit of masonry structures. In *Proceedings of the 3rd International Conference on Protection of Historical Constructions* (Mazzolani FM, Lamas A, Calado L, Proenca JM and Faggiano B (eds)). IST Press, Lisbon, Portugal

Goodwin C, Tonks G and Ingham J (2011) Retrofit techniques for seismic improvement of URM buildings. *SESOC Journal* **24(1)**: 16.

Kaushik HB, Rai DC and Jain SK (2007) Stress-strain characteristics of clay brick masonry under uniaxial compression. *Journal of Materials in Civil Engineering* **19(9)**: 728–739.

Kouris LAS and Triantafillou TC (2018) State-of-the-art on strengthening of masonry structures with textile reinforced mortar (TRM). *Construction and Building Materials* **188**: 1221–1233, https://doi.org/10.1016/j.conbuildmat.2018.08.039.

Lin YW, Wotherspoon L, Scott A and Ingham JM (2014) In-plane strengthening of clay brick unreinforced masonry wallettes using ECC shotcrete. *Engineering Structures* **66**: 57–65.

Lin Y, Lawley D, Wotherspoon L and Ingham JM (2016) Out-of-plane testing of unreinforced masonry walls strengthened using ECC shotcrete structures. *Structures* **7**: 33–42, https://doi.org/10.1016/j.istruc.2016.04.005.

Lucchini A, Mazzucchelli ES, Mangialardo S and Persello M (2014) Façadism and CLT technology: An innovative system for masonry construction refurbishment. *Proceedings of the 40th IAHS World Congress on Housing, Funchal, Portugal.*

Lumantarna R (2012) *Material Characterisation of New Zealand's Unreinforced Masonry Buildings*. Doctoral dissertation, The University of Auckland, Auckland, New Zealand.

NZSEE (New Zealand Society for Earthquake Engineering) (2017) *The Seismic Assessment of Existing Buildings. Part C8: Seismic Assessment of Unreinforced Masonry Buildings*. NZSEE, Wellington, New Zealand.

Miglietta M, Damiani N, Grottoli L, Guerrini G and Graziotti F (2019) Shake-table investigation of a timber retrofit solution for unreinforced masonry cavity-wall buildings. *Proceedings of XVIII Convegno Anidis, Ascoli Piceno, Italy*. Pisa University Press, Pisa, Italy, pp. 117–127.

MIT (Ministero Delle Infrastrutture e dei Trasporti) (2019) *C.S.LL.PP. N°7: Istruzioni per L'applicazione Dell<<Aggiornamento delle "Norme Tecniche per le Costruzioni">> di cui al decreto ministeriale 17 gennaio 2018*. MIT, Rome, Italy (in Italian).

Morandi P, Albanesi L, Graziotti F *et al.* (2018) Development of a dataset on the in-plane experimental response of URM Piers with bricks and blocks. *Construction and Building Materials* **190**: 593–611, https://doi.org/10.1016/j.conbuildmat.2018.09.070.

OIB (Österreichisches Institut für Bautechnik) (2018) *ETA-18/0303:* Rubner XLAM – Rubner CL. Solid wood slab elements to be used as structural elements in buildings. OIB, Vienna, Austria.

Riccadonna D, Giongo I, Schiro G, Rizzi E and Parisi MA (2019) Experimental shear testing of timber-masonry dry connections for the seismic retrofit of unreinforced masonry shear walls. *Construction and Building Materials* **211**: 52–72, https://doi.org/10.1016/j.conbuildmat.2019.03.145.

Robertson A, Lam F and Cole R (2012) A comparative cradle-to-gate life cycle assessment of mid-rise office building construction alternatives: laminated timber or reinforced concrete. *Buildings* **2**: 245–270.

Sustersic I and Dujic B (2014) Seismic shaking table testing of a reinforced concrete frame with masonry infill strenghtened with cross laminated timber panels. In *Proceedings of the World Conference on Timber Engineering, Quebec, QC, Canada*.

Tomasi R and Sartori T (2013) Mechanical behaviour of connections between wood framed shear walls and foundations under monotonic and cyclic load. *Construction and Building Materials* **44(13)**: 682–690, https://doi.org/10.1016/j.conbuildmat.2013.02.055.

Valek J and Veiga R (2005) Characterisation of mechanical properties of historic mortars – testing of irregular samples. In *Structural Studies, Repairs and Maintenance of Heritage Architecture XI* (Brebbia CA and Torpiano A (eds)). WIT Press, Southampton, UK, pp. 365–374.

Wang C, Sarhosis V and Nikitas N (2018) Strengthening/retrofitting techniques on unreinforced masonry structure/element subjected to seismic loads: a literature review. *The Open Construction and Building Technology Journal* **12(1)**: 251–268.

How can you contribute?

To discuss this paper, please email up to 500 words to the editor at journals@ice.org.uk. Your contribution will be forwarded to the author(s) for a reply and, if considered appropriate by the editorial board, it will be published as discussion in a future issue of the journal.

Proceedings journals rely entirely on contributions from the civil engineering profession (and allied disciplines). Information about how to submit your paper online is available at www.icevirtuallibrary.com/page/authors, where you will also find detailed author guidelines.